IOP Publishing Nanotechnology
Nanotechnology 27 (2016) 125702 (8pp) doi:10.1088/0957-4484/27/12/125702

Tip-induced gating of molecular levels in carbene-based junctions

Giuseppe Foti and Héctor Vázquez

Institute of Physics, Academy of Sciences of the Czech Republic, Cukrovarnicka 10, Prague, Czech Republic

E-mail: foti@fzu.cz and vazquez@fzu.cz

Received 13 November 2015, revised 22 January 2016
Accepted for publication 29 January 2016
Published 18 February 2016

Abstract

We study the conductance of N-heterocyclic carbene-based (NHC) molecules on gold by means of first-principles calculations based on density-functional theory and non-equilibrium Green's functions. We consider several tip structures and find a strong dependence of the position of the NHC molecular levels with the atomistic structure of the tip. The position of the lowest unoccupied molecular orbital (LUMO) can change by almost 0.8 eV with tip shape. Through an analysis of the net charge transfer, electron redistribution and work function for each tip structure, we rationalize the LUMO shifts in terms of the sum of the work function and the maximum electrostatic potential arising from charge rearrangement. These differences in the LUMO position, effectively gating the molecular levels, result in large conductance variations. These findings open the way to modulating the conductance of NHC-based molecular circuits through the controlled design of the tip atomistic structure.

Keywords: single molecule transport, N-heterocyclic carbene, tip-induced gating, DFT–NEGF, metal-molecule charge rearrangement

(Some figures may appear in colour only in the online journal)

1. Introduction

The extremely broad tailoring capabilities of chemical design have stimulated a strong research effort in the field of molecular electronics [1–3]. The conducting properties of single molecules placed between two electrodes have been explored from both theory and experiment and have been found to depend sensitively on several chemical and structural factors such as molecular backbone structure and conformation [4–7], molecular length [8–11], tilt-angle [12–14], anchoring groups [15–17] and electrode material [16–19], among others. In particular, at the molecular scale the actual conformation of the metallic contacts to the molecules drastically affects conductance [20–27]. This not only introduces an additional source of variability that is not always easy to measure or control experimentally [15–17], but could also have important implications for heat dissipation and thermal stability of the molecular junction [28]. Therefore studies of the effect of electrode shape are an important step in fully understanding the electronic and conducting properties of molecular junctions.

In break-junction conductance measurements [15–17, 19, 29] the junction is repeatedly broken and re-formed and the atomistic details of the metal-molecule contacts are not known. At the same time, in low temperature and ultra-high vacuum conditions, control over the tip structure can be achieved. Atomic clusters with different shapes can be assembled by lateral manipulation of the atoms deposited on the electrode surface [26, 30].

First-principles simulations are a powerful tool with which to study the electronic structure and conductance of molecular junctions, where the atomistic details of the junction are properly taken into account [1, 2]. In this paper we carry out density-functional theory (DFT) based conductance calculations of a molecular junction and focus on the effect of tip structure. We consider a carbene-based molecule whose frontier orbitals are seen to shift strongly with changes in the tip structure.

NHCs [31] have attracted a lot of attention for their interesting properties and broad range of applications [32]. NHCs are strong σ donors, exhibit high reactivity and are extensively used as ligands in transition-metal catalysts and

stabilizing agents for metallic nanoparticles [33]. On gold, NHCs have shown interesting luminescence properties [34] and ultra-stable chemical and thermal properties [35]. The binding of NHCs to Au is particularly interesting for single molecule transport since covalent Au–C metal-molecule bonds were shown to result in highly-conducting properties [36–39].

In this paper we therefore investigate the conducting properties of NHC-based junctions with different tip terminations using DFT and non-equilibrium Green's functions (NEGF). DFT-based calculated conductance values typically overestimate those reported in experiment. Corrections to the calculated resonance positions bring the calculated conductance closer to experiment [23, 40–43]. Here we focus instead on the effect of the atomistic structure of the tip on NHC-based junctions. The changes in frontier orbital position across the different tips are explained in terms of electrostatic effects at the junction, as detailed below. Therefore we believe this trend to be well represented within DFT. Previous studies, based on charge-transfer, addressed the tip dependence of molecular levels position for the weakly coupled bipyridine molecule [44, 45]. Here we show that for the NHC-based junction, characterized by strong metal-molecule bonds, a study of the electron density redistribution associated to the metal-molecule interaction characterizes the shift of molecular levels for each electrode termination. These tip-induced shifts in the positions of frontier orbitals effectively gate the NHC-based molecular circuit.

2. Geometries and computational details

We calculate the conducting properties of carbene-like molecules anchored to Au(100) through several tips structures. These molecules are NHCs consisting of a central conjugated ring with imidazole terminations which form bonds to the Au tips. We consider four different tip structures which are meant to model some of the different tip geometries which can be formed in break junction or engineered in LT-UHV experiments. The simplest tip consists of a gold adatom (A) adsorbed on the surface. The tetrameric tip (T) has four atoms corresponding to the Au(100) positions. The pyramidal tip (P) consists of a Au atom on top of a tetramer. Finally we consider a structure (C) where a Au atom is situated on top of a pyramidal tip forming a chain-like structure. This last geometry is motivated by the strength of the Au–C bond and by the results of simulations where the molecule is pulled from the surface, where the Au–Au, rather than the Au–C bond, is found to break [46]. In all cases, junction geometries are relaxed, as described below, and we find that the molecule binds above the terminal tip apex. In the case of the tetrameric tip, the molecule binds above one of the corners and there is some bending of the conjugated backbone due to the interaction of the π backbone. Figure 1 shows the junction geometries as well as details of the tip structures (insets).

We use Siesta [47] and TranSiesta [48] for the structure relaxation and the calculation of the electronic and transport properties. We use a single-ζ plus polarization basis for gold and a double-ζ plus polarization basis for nitrogen, hydrogen and carbon atoms. Exchange-correlation is described with the generalized gradient approximation [49].

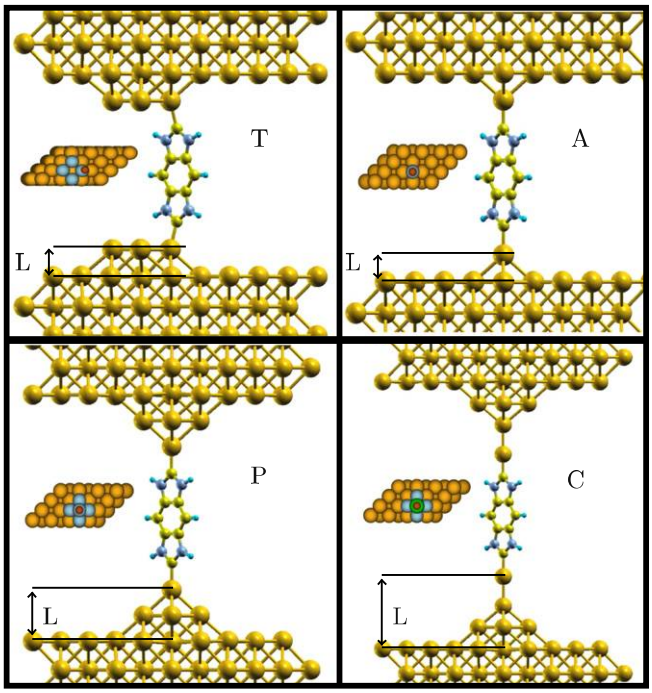

Figure 1. The four tip geometries considered: tetramer (T), adatom (A), pyramid (P) and chain-like structure (C). Insets show a top view of the Au slab (orange), Au tip atoms (blue) and the first C atom (brown). In the case of the C geometry, the Au atom above the pyramidal structure is shown in green.

We carry out all transport calculations at representative geometries obtained by minimizing the energy with respect to the inter-electrode separation. The position of the molecule, tip atoms and the first gold layer were relaxed until residual forces fell below 0.02 eV Å^{-1}. We use a $k = 5 \times 5$ Monkhorst–Pack grid for the calculation of the electronic structure and a $k = 15 \times 15$ grid for transmission spectra. Eigenchannels are calculated following the method of Paulsson and Brandbyge [50] using Inelastica [51].

3. Results

Figure 2 shows the electron transmission spectra $T(E)$ of the NHC-based molecule with the four tip structures considered.

3.1. Elastic transmission

At energies close to those of molecular backbone resonances, the spectra show peaks with a transmission close to 1. Below the edge of the Au d band situated at ~ -2 eV, the molecular states are in resonance with these states and result in high-transmission features in the $T(E)$ curves. A clear trend is apparent from figure 2, where the curves are shifted with respect to each other, with the spectral features appearing at progressively deeper energies along the T, A, P and C tip series. This is also clearly reflected in the position of the

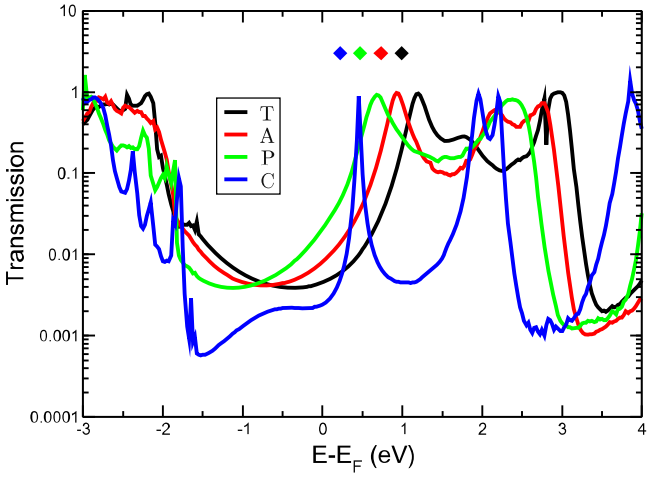

Figure 2. Transmission spectra and position of the MPSH LUMO (diamonds) for the geometries considered.

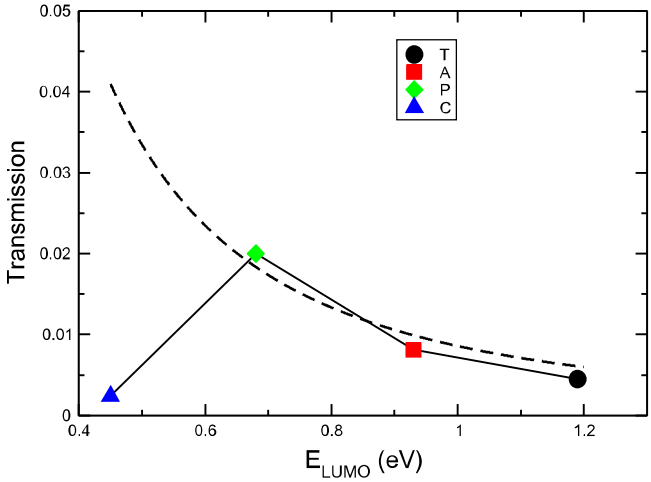

Figure 3. Transmission at the Fermi level as a function of LUMO peak position for the structures considered. The dashed line represents the transmission for a one-level model centered at E_{LUMO} with a constant FWHM Γ_{av} given by the average of the T, A and P values, as described in the text.

Table 1. Position of the LUMO peak, conductance at the Fermi level, full width at half maximum Γ of the LUMO resonance and net charge on the molecule ΔQ for all tip structures.

Tip	E_{LUMO} (eV)	G(E_{F}) (G_0)	Γ (eV)	ΔQ (−e)
T	1.19	0.0045	0.16	−0.37
A	0.93	0.0081	0.18	−0.50
P	0.68	0.0200	0.22	−0.45
C	0.45	0.0024	0.03	−0.41

eigenstates of the molecular projected self-consistent Hamiltonian (MPSH) shown in figure 2 as filled diamonds. The MPSH is constructed for each junction as the 'box' in the metal/molecule/metal Hamiltonian corresponding to the molecular region only. It differs from the Hamiltonian of an isolated molecule with the same geometry in that the MPSH matrix elements are those of the molecule at the junction. Other MPSH empty orbitals follow the same trend.

The LUMO-derived resonance plays a dominant role for all tip structures. Its calculated position changes over ∼0.75 eV with the choice of tip structure, from 1.19 eV for the tetramer to 0.45 eV for the chain-like tip. While variations in the position of molecular level resonances with tip shape have been previously reported for other molecular junctions, we note that these were smaller, typically $\lesssim$0.5 eV [20, 23, 25, 27].

For the first three tip structures (T, A, P) this shift results in an increase of the calculated conductance, from $4.5 \times 10^{-3} G_0$ to $2.0 \times 10^{-2} G_0$ (table 1). However, the calculated conductance of the chain-like tip structure (C) is much lower ($2.4 \times 10^{-3} G_0$) despite the LUMO position closer to the Fermi level. This latter value results from the lower electronic coupling in the chain-like structure where the molecule is physically separated from the electrode and tip structures. Table 1 shows the full width at half maximum of the LUMO resonance, calculated from Lorentzian fits of the transmission peak. The width is roughly the same for the T, A and P tip structures but much smaller for C. In order to calculate the conductance reduction arising from the reduced coupling in the chain-like structure and disentangle the effects of the LUMO position from the electronic coupling, we average the width of the LUMO peak for the T, A and P structures. This value $\Gamma_{\mathrm{av}} = 0.19$ eV gives an estimate of the electronic coupling of non-chain-like tip geometries. Figure 3 shows the calculated zero-bias conductance across the T, A, P, C series as a function of the LUMO position. The dashed line shows the transmission at the Fermi level as a function of E_{LUMO} of a one-level system [2] having a broadening given by Γ_{av}. For the T, A and P structures, the dashed line is close to the calculated conductance values, implying that these tip structures are well described by a simple one-level model with a constant (averaged) width. For the chain-like C structure there is a large discrepancy in the conductance calculated from the one-level model and from first-principles, the former being ∼17× higher. Therefore this comparison allows us to quantify the effect on conductance of the reduced electronic coupling of structure C. We note that the C geometry has a binding energy that is stronger than the other junctions by ≃0.3 eV, as expected from the undercoordinated Au atoms. However, for this elongated structure, this reduced coordination of the contact Au atom results in smaller hybridization and decouples the molecular states from the bulk, resulting in narrower spectral features of the C structure.

Despite the smaller electronic coupling of the molecular states in the C geometry, the nature of the conducting orbitals is the same for all four tip structures considered. The LUMO peak corresponds to an orbital of π symmetry delocalized over the whole molecular backbone. This is the also case for other unit transmission peaks in figure 2. In addition to these π peaks, there is a channel of σ symmetry involving mostly Au tip atoms and the imidazole end group, whose transmission varies slowly over several eVs around the Fermi level. Figure 4 shows these two transmission channels for adatom tips (A). The figure shows the real part of the scattering state

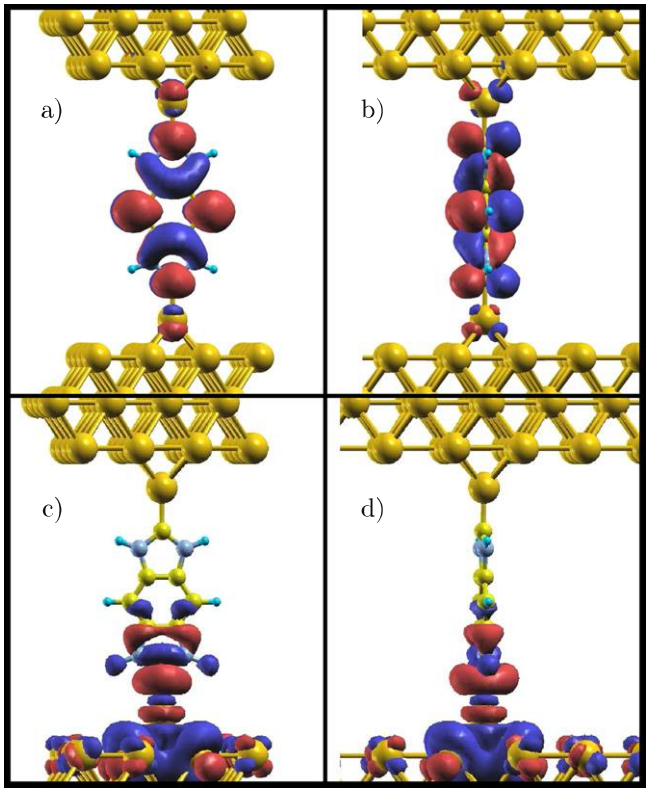

Figure 4. (a)–(b) First and (c)–(d) second most transmitting eigenchannels at the energy of the LUMO peak for the A geometry, having π and σ-type symmetry, respectively.

of the most conducting (π) and second most conducting (σ) channels at the energy of the LUMO resonance for isovalues of 0.05 and 0.01 e Bohr^{-3} respectively. Away from molecular backbone resonances the conductance of this π channel decreases. Depending mostly on the width of these peaks, the transmission of this channel can fall below the transmission of the σ channel either at some energies or at certain k-points. This is the case (figure 2) of the C geometry between −1.5 and 0 eV, where the most conducting channel is the σ channel.

3.2. Molecular level shift: electrostatic effects

The dependence of frontier energy level position with tip shape depends on the atomistic details of the interface and on the electronic properties of both metal and molecule. The work function for the specific electrode termination, its initial offset to the isolated molecular levels, the spatial distribution of these states and the junction geometry all determine the charge transfer and rearrangement that takes place at the interface. Different mechanisms that contribute to the interface dipoles such as the formation of metal-molecule chemical bonds, compression of the metal wave functions upon adsorption ('pillow effect') or molecular permanent dipoles, have been studied [52]. In these NHC junctions, the molecular level shift due to the coupling to the electrodes is, from the MPSH eigenstates in figure 2, approximately the same for all structures (~0.2 eV) and corresponds to an up-shift with respect to the isolated molecule. Thus this effect cannot on its own explain the relative position of the LUMO peak for the four different junctions, requiring an analysis of the level alignment including electrostatic effects of metal-molecule interactions. The position of molecular resonances for different tip shapes was analyzed in detail in the past for bipyridine on Au [20, 44, 45]. There, the authors observed large changes in the LUMO position with tip shape and established a relation between its position and the coordination number N_c of the gold atom in contact with the molecule. The authors highlighted the role of the metal d states and explained the shift of molecular levels in terms of metal-molecule charge transfer. We also investigated the role of the metal d states but found no clear correlation. Instead, we find that our results can be clearly understood in terms of charge redistribution and change in the work function for the different electrode terminations.

Upon adsorption, charge transfer and rearrangement result in the renormalization of molecular levels with respect to the isolated molecule [52]. The charge redistribution associated to such process is commonly discussed in terms of the plane-averaged difference between the electron density of the molecular junction and that of the isolated metal and molecular subsystems [53, 54]:

$$\overline{\rho}_{\mathrm{diff}}(z) = \overline{\rho}_{\mathrm{jcn}}(z) - [\overline{\rho}_{\mathrm{mol}}(z) + \overline{\rho}_{\mathrm{metal}}(z)], \qquad (1)$$

where $\overline{\rho}_{\mathrm{jcn}}(z)$ is the electron density of the metal/molecule/metal junction while $\overline{\rho}_{\mathrm{mol}}(z)$ and $\overline{\rho}_{\mathrm{metal}}(z)$ are the electron densities for the isolated molecule and metal subsystem, respectively. This approach takes into account the combined effect due to charge transfer and redistribution at the junction. In the calculation of the charge densities of both subsystems we used ghost orbitals in order to correct for basis-set superposition errors [55].

The plane-averaged electron redistribution $\overline{\rho}_{\mathrm{diff}}(z)$ is shown in figure 5. Inside the molecule $\overline{\rho}_{\mathrm{diff}}(z)$ is negative, corresponding to electron depletion, and approximately the same for all four junctions; the most relevant differences arise in the region corresponding to the tip atoms. In all cases there is an electron accumulation on Au atoms; the maximum electron density increase of all four junctions is 0.34$|e|$ Å^{-1} near the surface Au layer in the A geometry. In all cases this charge redistribution is almost completely screened out at the second gold layer.

Table 1 shows the net charge of the molecule, calculated by integrating equation (1) in the z-direction. Due to the sharp oscillations of $\overline{\rho}_{\mathrm{diff}}$ [44, 53, 56], ΔQ is sensitive to the choice of the boundary points for integration. Here we choose the Au–C midpoints, in agreement with other works [56, 57].

The net charge transfer is strong and negative, corresponding to electron transfer from molecule to Au, consistent with the reported donor behavior of carbenes [32]. Nevertheless, regardless of the integration limits for the calculation of ΔQ, there is no clear relation between the LUMO position and ΔQ and molecular level position cannot be fully explained in terms of net charge transfer alone.

The electric field and electrostatic potential associated with charge rearrangement upon adsorption across the molecular junction can be obtained by solving the one-dimensional Poisson equation for the plane-averaged

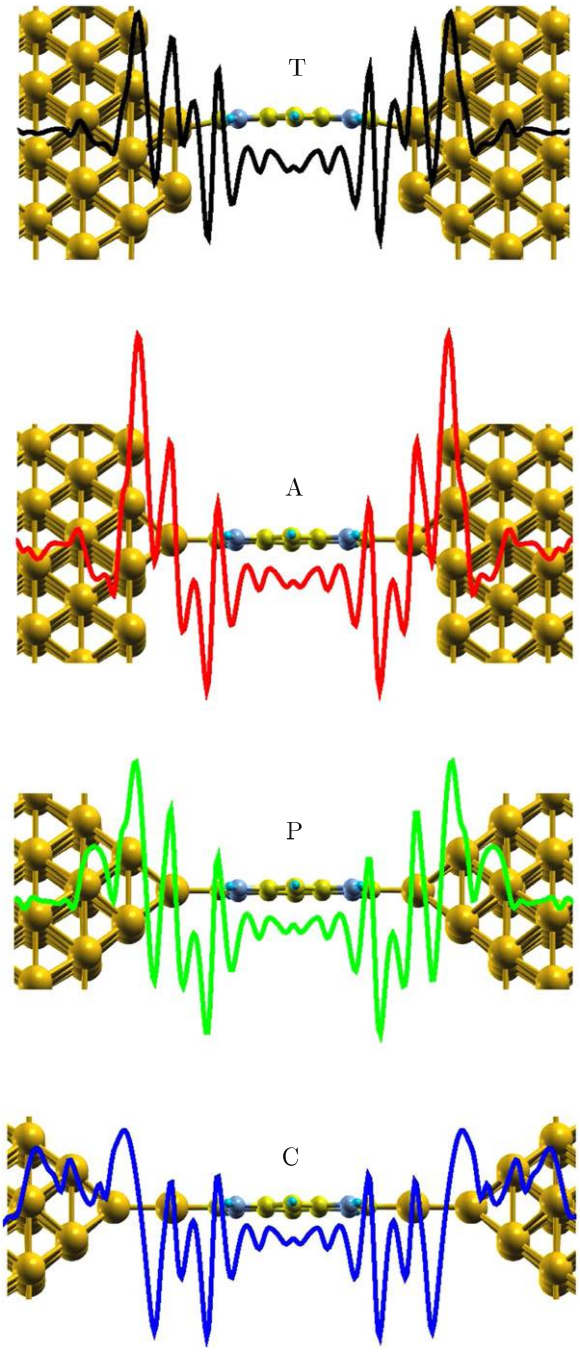

Figure 5. Plane-averaged electron density differences $\overline{\rho}_{\rm diff}$ and the corresponding junction geometries. Electrons are depleted from the molecular region in all four cases.

charge density difference:

$$\nabla E\,(z) = \frac{e\overline{\rho}_{\rm diff}\,(z)}{\epsilon_0}. \qquad (2)$$

Here we used the vacuum dielectric constant ϵ_0. Figure 6 shows the electric field across the junction for all structures. The field reaches its maximum amplitude close to both metal-molecule interfaces and goes to zero at the center of the molecule. The overall shape as a function of the distance along the z-direction approximately resembles two triangles. Figure 6 also shows vertical lines near both interfaces where

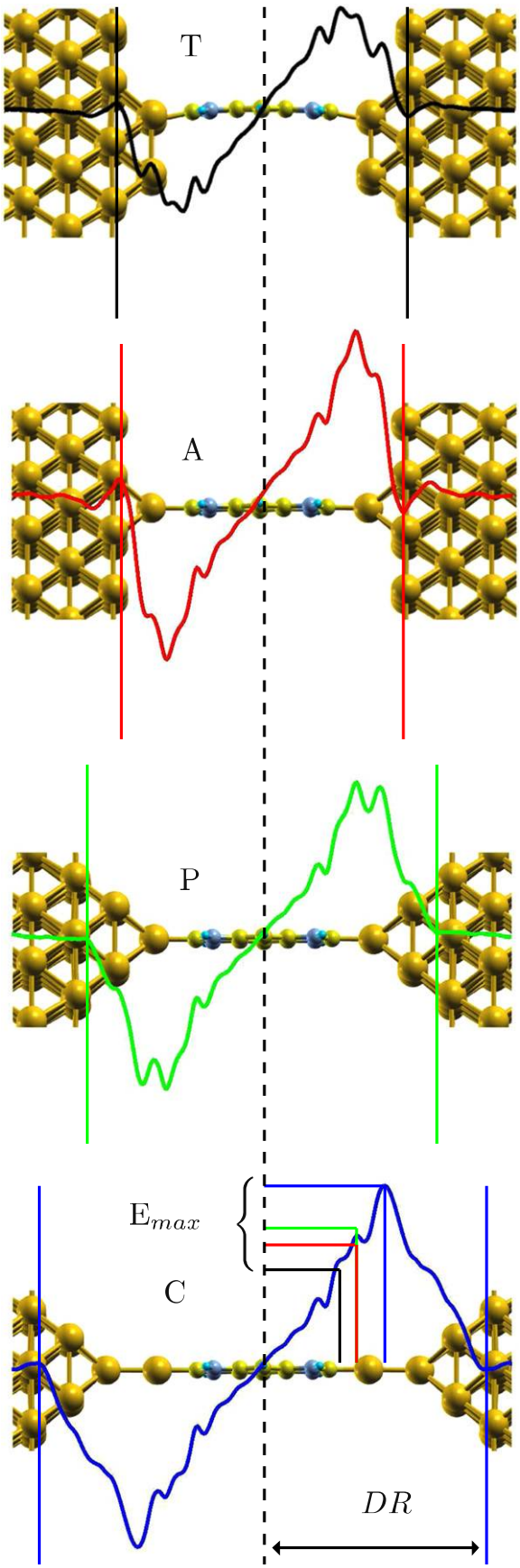

Figure 6. Electric field $E(z)$ across the junction for all structures. Vertical lines delimit the depletion region (DR). The lower panel compares the maximum values of the electric field in all four cases.

Table 2. Coordination number N_c of the tip contact atom, maximum electric field E_{max}, length of the tip, extension of the depletion region *DR*, maximum of the renormalization potential energy and tip work function for all tip structures.

N_c	E_{max} (V/Å)	L (Å)	DR (Å)	eV_{max} (eV)	Φ_t (eV)
T(6)	0.25	1.96	7.57	−1.00	5.27
A(4)	0.40	1.88	7.47	−1.38	5.38
P(4)	0.38	3.90	9.30	−1.65	5.24
C(1)	0.45	6.42	11.83	−2.35	5.60

the field reaches a minimum value. This depletion region (DR) effectively indicates where in the junction an induced field arises due to charge rearrangement. The extension of the DR depends on the tip structure. If we measure tip length as the vertical distance of the contact Au atom from the Au surface layer (figure 1), DR is larger for longer tips, as shown in table 2. Finally, the bottom panel of figure 6 compares the maximum amplitudes E_{max} of the induced electric field for all four cases. Interestingly, E_{max} is higher for the tips where the tip contact atom has a lower coordination number N_c (table 2).

The two parameters E_{max} and DR define the amplitude of the electrostatic potential profile $V(z)$ felt by the electrons tunneling through the junction. $V(z)$ is obtained by integrating the electric field along the z-direction and corresponds to the potential resulting from the charge redistribution at the junction:

$$V(z) = -\int_{-\infty}^{z} E(z)\mathrm{d}z. \quad (3)$$

Larger E_{max} and DR values result in a larger maximal renormalization potential amplitude V_{max}. The maximum values of the electrostatic potential energy profiles are listed in table 2. For all geometries, the renormalization potential energy $eV(z)$ is negative, consistent with a downshift of molecular levels with respect to the isolated molecule due to charge transfer and redistribution. The maximum amplitude of this renormalization potential V_{max} is larger for longer tips and for lower N_c. These results suggest that atomic scale design of tip structure in NHC-based junctions can allow control over the position of molecular levels, and in particular the LUMO, over several tenths of an eV.

The trend of eV_{max} with tip shape is consistent with the downshift of the LUMO peak position in the transmission spectra. Nevertheless the LUMO position does not depend linearly on eV_{max} either. The relation of the LUMO position with respect to tip shape is understood when one includes in the analysis the work function Φ_t of the different Au structures, where the values Φ_t depend on the specific tip termination. The calculated values of Φ_t are listed[1] in table 2. The

[1] To calculate the work function corresponding to each tip termination in SIESTA we first compute the Fermi level in a separate bulk electrode calculation. We then remove all molecular atoms from the metal/molecule/metal structure. Φ_t is the bulk Fermi level modified by the difference of the electrostatic potential, corrected by the neutral atom potential, in the plateaus inside the metal and at the center of the vacuum gap for each metal/vacuum/metal junction [59].

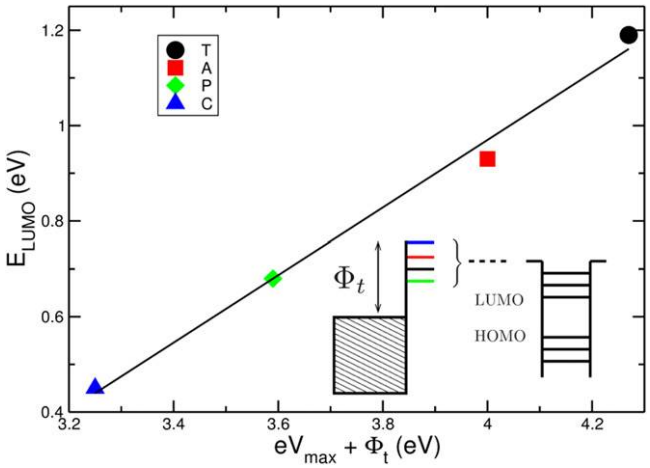

Figure 7. Position of the LUMO peak as a function of the sum of the local work function Φ_t and the maximum renormalization potential energy eV_{max}. The inset illustrates the molecular levels tending to align with the work function of the specific tip structure.

values for the T, A and P geometries are close to that of the flat surface (5.37 eV) and close to experiment [58]. For the chain-like geometry C we get a larger value of 5.6 eV. Φ_t determines the local potential with which the orbitals of the NHC molecule tend to align (inset in figure 7). The values of Φ_t reflect the slightly different surface dipoles and potential energy profiles in the proximity of the surface. The charge rearrangement at the interface $\overline{\rho}_{diff}(z)$, on the other hand, is associated to metal-molecule interactions and can be expected to result in different potential energy profiles $eV(z)$ for each particular junction. The sum of the work function for each tip structure Φ_t with the potential energy at the center of the molecule eV_{max}, thus defines the shift in the position of the LUMO across the different junctions. Figure 7 shows a clear linear relation between the LUMO position and $\Phi_t + eV_{max}$, which completely characterizes the charge rearrangement at each junction. A similar result, where the level shifts increase with a decreasing coordination number, had been reported for the weakly coupled bipyridine/Au system [45]. For NHC-gold junctions, where we observe a strong dependence of the LUMO position with tip shape, the atomistic details of tip termination strongly influence the level alignment. Thus, our results provide a complementary direction for the gating of NHC-based molecular circuits.

4. Conclusions

In this paper we have studied the electronic and transport properties of a NHC-based molecule anchored to Au(100) through a series of tips of different shape. In particular we considered tips consisting of an adatom, a tetramer, a pyramid and a chain-like termination where a Au atom is positioned above a pyramidal tip. We found that for these NHC-based junctions the atomistic details of the tip structure strongly influence the position of molecular levels, in particular of the LUMO, which can change over almost 0.8 eV and which

determines conductance. We completely characterized the LUMO position in terms of the electrostatics involved in the charge rearrangement at each junction. Although the total transferred charge, charge redistribution and work function are different from one junction to another, the LUMO position cannot be explained in terms of these quantities alone. Instead, we found that the LUMO shifts correlate closely with the sum of two quantities which depend on the specific tip structure: the work function and the maximum electrostatic potential arising from charge rearrangement. These terms describe respectively the different initial situations for alignment (e.g. work function) and the charge redistribution at the junction associated to the alignment process. Longer tips with a low coordination number of the Au atom which binds to the molecule induce a more pronounced downshift of molecular levels. Since transport is LUMO-dominated, this downshift results in a conductance increase except for the chain-like tip where, despite the strongest downshift, the significantly weaker electronic coupling decreases conductance. Our results show that the choice of tip structure, by determining the LUMO position, effectively gates the carbene levels. This opens the way for the tuning of conductance in NHC-based molecular junctions through the controlled design of tip structure.

Acknowledgments

We gratefully acknowledge financial support from the Czech Science Agency (GAČR) under project 15-19672S, the Academy of Sciences of the Czech Republic and the Purkyně Fellowship program. Computational resources were provided by MetaCentrum under the program LM2010005 and CERIT-SC under the program Centre CERIT Scientific Cloud, part of the Operational Program Research and Development for Innovations, Reg. no. CZ.1.05/3.2.00/08.0144.

References

[1] Cuniberti G, Fagas G and Richter K (ed) 2005 *Introducing Molecular Electronics: A Brief Overview* (Berlin: Springer)
[2] Cuevas J C and Scheer E 2010 *Molecular Electronics: An Introduction to Theory and Experiment* (Singapore: World Scientific)
[3] Ratner M 2013 *Nat. Nanotechnol.* **8** 378
[4] Donhauser Z J *et al* 2001 *Science* **292** 2303
[5] Venkataraman L, Klare J E, Nuckolls C, Hybertsen M S and Steigerwald M L 2006 *Nature* **442** 904
[6] Chen L, Pobelov I, Wandlowski T, Bagrets A, Arnold A and Evers F 2008 *J. Am. Chem. Soc.* **130** 318
[7] Mishchenko A *et al* 2010 *Nano Lett.* **10** 156
[8] Wang W, Lee T and Reed M A 2003 *Phys. Rev.* B **68** 035416
[9] Beebe J M, Engelkes V B, Jingquan L, Gooding J J, Eggers P K, Jun Y, Zhu X, Paddon-Row M N and Frisbie C D 2005 *J. Phys. Chem.* B **109** 5207
[10] Li X, He J, Hihath J, Xu B, Lindsay S M and Tao N 2006 *J. Am. Chem. Soc.* **128** 2135
[11] Lu Q, Liu K, Zhang H, Du Z, Wang X and Wang F 2009 *ACS Nano* **3** 3861
[12] Haiss W, Wang C, Grace I, Batsanov A S, Schiffrin D J, Higgins S J, Bryce M R, Lambert C J and Nichols R J 2006 *Nat. Mater.* **5** 995
[13] Quek S Y, Kamenetska M, Steigerwald M L, Choi H J, Louie S G, Hybertsen M S, Neaton J B and Venkataraman L 2009 *Nat. Nanotechnol.* **4** 230
[14] Smaali K, Desbief S, Foti G, Frederiksen T, Sanchez-Portal D, Arnau A, PNys J, Leclere P, Vuillaume D and Clement N 2015 *Nanoscale* **7** 1809
[15] Hihath J and Tao N 2014 *Semicond. Sci. Technol.* **29** 054007
[16] Sun L, Diaz-Fernandez Y A, Gschneidtner T A, Westerlund F, Lara-Avila S and Moth-Poulsen K 2014 *Chem. Soc. Rev.* **43** 7378
[17] Schwarz F and Lörtscher E 2014 *J. Phys.: Condens. Matter* **26** 474201
[18] Cho Y, YKim W and SKim K 2009 *J. Phys. Chem.* A **113** 4100
[19] Kiguchi M and Kaneko S 2013 *Phys. Chem. Chem. Phys.* **15** 2253
[20] Stadler R, Thygesen K S and Jacobsen K W 2005 *Phys. Rev.* B **72** 241401
[21] Müller K-H 2006 *Phys. Rev. B* **73** 045403
[22] Yan X-W, Liu R-J, Li Z-L, Zou B, Song X-N and Wang C-K 2006 *Chem. Phys. Lett.* **429** 225
[23] Quek S Y, Venkataraman L, Choi H J, Louie S G, Hybertsen M S and Neaton J B 2007 *Nano Lett.* **7** 3477
[24] Shukla M K, Dubey M and Leszczynski J 2008 *ACS Nano* **2** 227
[25] Zhang R, Ma G, Bai M, Sun L, Rungger I, Shen Z, Sanvito S and Hou S 2010 *Nanotechnology* **21** 155203
[26] Schull G, Frederiksen T, Arnau A, Sánchez-Portal D and Berndt R 2011 *Nat. Nanotechnol.* **6** 23
[27] Bilan S, Zotti L A, Pauly F and Cuevas J C 2012 *Phys. Rev.* B **85** 205403
[28] Schulze G, Franke K J and Pascual J I 2008 *New J. Phys.* **10** 065005
[29] Xiang D, Jeong H, Lee T and Mayer D 2013 *Adv. Mater.* **25** 4845
[30] Wang Y F, Kröger J, Berndt R, Vázquez H, Brandbyge M and Paulsson M 2010 *Phys. Rev. Lett.* **104** 176802
[31] Arduengo A J III, Harlow R L and Kline M 1991 *J. Am. Chem. Soc.* **113** 361
[32] Hopkinson M N, Richter C, Schedler M and Glorius F 2014 *Nature* **510** 485
[33] Díez-González S, Marion N and Nolan S P 2009 *Chem. Rev.* **109** 3612
[34] Visbal R, Ospino I, López-de-Luzuriaga J M, Laguna A and Gimeno M C 2013 *J. Am. Chem. Soc.* **135** 4712
[35] Crudden C M *et al* 2014 *Nat. Chem.* **6** 409
[36] Cheng Z-L, Skouta R, Vázquez H, Widawsky J, Schneebeli S, Chen L W S, Hybertsen M, Breslow R and Venkataraman L 2011 *Nat. Nanotechnol.* **6** 353
[37] Chen W, Widawsky J R, Vázquez H, Schneebeli S T, Hybertsen M S, Breslow R and Venkataraman L 2011 *J. Am. Chem. Soc.* **133** 17160
[38] Widawsky J R, Chen W, Vázquez H, Kim T, Breslow R, Hybertsen M S and Venkataraman L 2013 *Nano Lett.* **13** 2889
[39] Foti G, Vázquez H, Sánchez-Portal D, Arnau A and Frederiksen T 2014 *J. Phys. Chem.* C **118** 27106
[40] Delaney P and Greer J C 2004 *Phys. Rev. Lett.* **93** 036805
[41] Koentopp M, Burke K and Evers F 2006 *Phys. Rev.* B **73** 121403
[42] Toher C and Sanvito S 2008 *Phys. Rev.* B **77** 155402
[43] Thygesen K S and Rubio A 2009 *Phys. Rev. Lett.* **102** 046802
[44] Stadler R and Jacobsen K W 2006 *Phys. Rev.* B **74** 161405

[45] Stadler R 2007 *J. Phys. Conf. Ser.* **61** 1097
[46] Vázquez H Mechanical and conducting properties of carbene-based molecular junctions (in preparation)
[47] Soler J M, Artacho E, DGale J, García A, Junquera J, Ordejón P and Sánchez-Portal D 2002 *J. Phys.: Condens. Matter* **14** 2745
[48] Brandbyge M, Mozos J-L, Ordejón P, Taylor J and Stokbro K 2002 *Phys. Rev.* B **65** 165401
[49] Perdew J P, Burke K and Ernzerhof M 1996 *Phys. Rev. Lett.* **77** 3865
[50] Paulsson M and Brandbyge M 2007 *Phys. Rev.* B **76** 115117
[51] Frederiksen T, Paulsson M, Brandbyge M and Jauho A-P 2007 *Phys. Rev.* B **75** 205413
[52] Ishii H, Sugiyama K, Ito E and Seki K 1999 *Adv. Mater.* **11** 605
[53] Heimel G, Romaner L, Zojer E and Brédas J-L 2007 *Nano Lett.* **7** 932
[54] Obersteiner V, Egger D A and Zojer E 2015 *J. Phys. Chem.* C **119** 21198
[55] van Duijneveldt F B, van Duijneveldt-van de Rijdt J G C M and van Lenthe J H 1994 *Chem. Rev.* **94** 1873
[56] Wang J-g, Prodan E, Car R and Selloni A 2008 *Phys. Rev.* B **77** 245443
[57] Peng G, Strange M, Thygesen K S and Mavrikakis M 2009 *J. Phys. Chem.* C **113** 20967
[58] Hansson G V and Flodström S A 1978 *Phys. Rev.* B **18** 1572
[59] Junquera J, Zimmer M, Ordejón P and Ghosez P 2003 *Phys. Rev.* B **67** 155327